King's Research Portal

Document Version
Peer reviewed version

Link to publication record in King's Research Portal

Cardiac hypoxia imaging:

second generation analogues of ^{64}Cu-ATSM

Maxwell G Handley, Rodolfo A Medina, Erika Mariotti,

Gavin D Kenny, Karen P Shaw, Ran Yan,

Thomas R Eykyn, Philip J Blower, Richard Southworth*

Imaging Sciences & Biomedical Engineering, King's College London.

maxwell.g.handley@kcl.ac.uk

richard.southworth@kcl.ac.uk. * Corresponding author

The Rayne Institute,

St. Thomas' Hospital,

Lambeth Palace Rd,

London. SE1 7EH

UK

Telephone +44 (0)207 1888374. Fax: +44 (0)207 1885442

4987 words

Running title: PET complexes for imaging hypoxia

Abstract

Myocardial hypoxia is an attractive target for diagnostic and prognostic imaging, but current approaches are insufficiently sensitive for clinical use. The PET tracer ^{64}Cu-ATSM has promise, but its selectivity and sensitivity could be improved by structural modification. We have therefore evaluated a range of ^{64}Cu-ATSM analogues for imaging hypoxic myocardium.

Methods: Isolated rat hearts (n=5/group) were perfused with normoxic buffer for 30 minutes, then hypoxic buffer for 45 minutes within a custom-built "triple γ-detector" system to quantify radiotracer infusion, hypoxia-dependent cardiac uptake, and washout. A 1 MBq bolus of each candidate tracer (and ^{18}FMISO for comparative purposes) was injected into the arterial line during normoxia, and early and late hypoxia, and their hypoxia selectivity and pharmacokinetics evaluated. The *in vivo* pharmacokinetics of promising candidates in healthy rats were then assessed by PET imaging and biodistribution.

Results: All analogues tested exhibited hypoxia sensitivity within 5 minutes. Complexes less lipophilic than ^{64}Cu-ATSM provided significant

gains in hypoxic:normoxic contrast (14:1 for ^{64}Cu-ATS, 17:1 for ^{64}Cu-CTS, 8:1 for ^{64}Cu-ATSM, $p<0.05$). Hypoxic first pass uptake was 78.2±7.2% for ^{64}Cu-ATS and 70.7±14.5% for ^{64}Cu-CTS, compared to 63.9±11.7% for ^{64}Cu-ATSM. *In vivo,* normoxic cardiac retention of ^{64}Cu-CTS was significantly lower than ^{64}Cu-ATSM and ^{64}Cu-ATS (0.13±0.02 versus 0.25±0.04 and 0.24±0.03% injected dose $p<0.05$), with retention of all three tracers falling to >0.7% injected dose within 6 minutes. ^{64}Cu-CTS also exhibited lower uptake in liver and lung.

Conclusion: ^{64}Cu-ATS and ^{64}Cu-CTS exhibit better cardiac hypoxia selectivity and imaging characteristics than the current lead hypoxia tracers ^{64}Cu-ATSM and [18]FMISO.

Key words: Hypoxia, PET, ^{64}Cu-ATSM, bis(thiosemicarbazones), [18]FMISO, cardiac ischemia

Introduction

Tissue hypoxia, as a facet of ischemia, is associated with many forms of cardiac dysfunction, including myocardial hibernation, non-compensated hypertrophy, microvascular disease, and heart failure.[1,2] Many of these conditions are difficult to identify or stratify using currently available technologies.[2, 3] To expand our window for anti-ischemic intervention, it would be desirable to non-invasively detect the disturbances in cardiac biochemistry which precede the functional and morphological changes that are currently identified by echocardiography, perfusion scintigraphy or MRI. Hypoxia-specific PET or SPECT radiotracers represent an opportunity to do this by identifying myocardial regions where oxygen demand exceeds supply, giving metabolic context to the more generic information gained by characterising deficits in either perfusion or contractility.[4]

While hypoxia-selective nitroimidazole derivatives like ^{18}F-fluoromisonidazole ([18]FMISO), and the non-nitroimidazole complex ^{99m}Tc-HL91, have been extensively investigated for applications in cancer imaging, their low first pass uptake, slow blood clearance and high liver uptake has meant that hypoxia imaging has failed to impact

4

significantly upon clinical practice in cardiology[3, 4]. The bis(thiosemicarbazone) (BTSC) complex ^{64}Cu-ATSM has been shown to selectively deposit radiocopper in hypoxic cultured cells,[5-9] isolated perfused hearts[10], *in vivo* in implanted tumours[11] and regionally ischemic myocardium in open chest dogs[12]. While it has been the subject of several promising clinical trials for applications in oncology,[13, 14] its utility for cardiovascular imaging has only been addressed in one very small clinical study of seven patients, with equivocal results.[15] Isolated cell studies suggest that ^{64}Cu-ATSM only accumulates in cells experiencing extracellular pO_2 below 1mm Hg[6], which, while suitable for identifying hypoxic tumours, may be more severely hypoxic than is typically evident in hypoxically compromised but salvageable myocardium. This may explain its mediocre performance in this small clinical trial.[3]

BTSC complexes are, however, highly modifiable in terms of redox potential and lipophilicity, with the potential to make them "tuneable" to different degrees of hypoxia for different applications or disease states. We have previously demonstrated the hypoxia selectivity of several complexes structurally related to ^{64}Cu-ATSM in isolated cancer cells *in vitro*[5, 6, 16], but they have yet to be evaluated for cardiac application, and

their relative pharmacokinetics in any dynamic model are currently unknown. In this study, we have therefore investigated the potential of these complexes for identifying hypoxic but viable myocardium. Using bi-exponential fitting of tracer washout curves in an isolated heart model, we describe the structure-activity relationships for a range of BTSCs, providing guidance for their future development for hypoxia imaging in general, and cardiovascular application in particular. We also present the first *in vivo* preclinical PET imaging, pharmacokinetic and biodistribution evaluations of two complexes that we have identified which exhibit better hypoxia selectivity than ^{64}Cu-ATSM.

Materials and Methods

Reagents and gas mixtures

All reagents were purchased from Sigma Aldrich (Poole, Dorset, UK) unless otherwise stated. All gas mixtures were purchased from BOC, UK. Specialist gas mixtures were certified by the manufacturer.

Animals

Male Wistar rats (220-240g, B&K Universal, UK) were used for all experiments. Animal procedures were in accordance with the Animals (Scientific Procedures) Act, UK. 1986.

Radionuclide production and ligand radiolabelling

^{64}Cu was produced at the Clinical PET Centre, St. Thomas' Hospital, London, UK as previously described. The structures of the BTSCs investigated are shown in Figure 1; their syntheses and radiolabelling protocol have also been reported previously[17,6]. [^{18}F]-fluoride was produced from the ^{18}O(p,n)^{18}F reaction by irradiation of [^{18}O]-water (97 atom%, Isochem Ltd., UK) with 11 MeV protons from a CTI RDS 112 cyclotron (beam current 30 μA). ^{18}FMISO was prepared following a previously reported method.[18]

Measurement of ^{64}Cu-BTSC retention factors and partition coefficients

1 µL of each ^{64}Cu-BTSC solution was pipetted onto an Instant Thin Layer Chromatography SG strip and developed using ethanol as the mobile phase. Strips were analysed using a Flow Count ITLC plate scanner, fitted with a $\beta^{-/+}$ detector (B-FC-3600, LabLogic, UK). Rf values and purities were determined using Laura software (v.4.0.3.75, Lablogic, UK). ^{64}Cu-BTSC partition coefficients were determined using H_2O or a modified Krebs-Henseleit Buffer (KHB, pH 7.4, detailed below) against octanol, as previously described.[19]

The triple γ-detection system

We developed a system for characterising the pharmacokinetics of radionuclide passage through an isolated perfused heart (Figure 2A), comprising three orthogonally oriented lead-collimated Na/I γ-detectors positioned (i) 3 cm downstream of a radiotracer injection port on the arterial line, 15 cm upstream of the heart cannula (to provide a radiotracer input function), (ii) directly opposite the heart itself, and (iii) over the venous outflow line (to provide an output function). Each was

8

connected to a modified GinaSTAR™ ITLC system running Gina™ software (Raytest Ltd, UK). Buffer oxygen saturation was monitored continuously by an in-line fluorescent oxygen/temperature probe inserted into the arterial line (Oxylab, Oxford Optronix UK Ltd).

Experimental protocol

Rats (n=5/group) were anesthetized with Sagatal (100 mg intraperitoneal), heparinized (200 IU intraperitoneal), and their hearts were excised and cannulated in the Langendorff mode as previously described.[20] They were perfused at 14 mL/min constant flow with KHB at 37°C containing: NaCl (118.5 mM), NaHCO$_3$ (25 mM), D-glucose (11 mM), KCl (8 mM), CaCl$_2$ (2.5 mM), MgSO$_4$ (1.2 mM) and Na$_2$EDTA (0.5 mM), gassed with 95% O$_2$ and 5% CO$_2$, and a left ventricular balloon used to measure contractile function.

After a 10 min stabilisation period, a bolus of radiotracer (1 MBq in 100 µL KHB) was injected into the arterial line. After 20 min, the perfusate was switched to hypoxic KHB from a parallel reservoir gassed with 95% N$_2$ and 5% CO$_2$. Further radiotracer boluses were administered 5 and 25 min after induction of hypoxia. Radiotracer flow through the perfusion

rig and heart was monitored by the triple γ-detector system. Coronary effluent was collected at regular intervals, and analysed for lactate content (by 2300 STAT Plus™ lactate analyser, YSI Ltd, UK) to identify the onset of anaerobic glycolysis, and creatine kinase (by standard spectrophotometric assay[21]) to monitor the extent of tissue necrosis.

Kinetic profiling of radiotracer retention and elution

Radiotracer time-activity curves were analysed with MATLAB® (MathWorks®, USA). Data were normalised to the maximum peak counts after each injection (as previously reported[22]), corrected for decay and background activity in the heart 30 seconds prior to each bolus injection. All washout curves described by *f(t)* were fitted to a bi-exponential function using least squares (Eq.1),

$$f(t) = a * e^{-b*t} + c * e^{-d*t} \qquad (1)$$

where *b* and *d* were the slow and fast clearance rate constants (SCR and FCR), and *a* and *c* were the respective weights of the SCR and FCR[22]. To evaluate goodness of fit, residuals at each time point were calculated (representative experimental datasets, overlaid fits and

residuals are presented in Figure 2C). Tissue retention was calculated as the residual activity in the heart 20 minutes post-injection as a percentage of the peak activity (% injected dose, %ID), as previously described.[10]

In vivo imaging and biodistributions

PET imaging was performed using a NanoPET-CT preclinical scanner (Mediso, Budapest, Hungary). Rats (n=3/group) were anesthetized with isofluorane, a CT scout scan was acquired, and dynamic PET scans covering the thorax were acquired for 30 minutes, with 6 MBq of either ^{64}Cu-ATSM, ^{64}Cu-CTS or ^{64}Cu-ATS injected intravenously one minute into the scan. CT images were then acquired using a 45 kVP X-ray source, 500 ms exposure time in 180 projections, using a pitch of 1.5 with an acquisition time of 5 mins to cover the thorax. A final whole body PET scan was then acquired to obtain biodistribution data (three bed positions, 10 minutes per position): 5 ns coincidence window; 400 – 600 keV energy window in 1:5 coincidence mode. Data were reconstructed using the following method: OSEM (6 subsets, 6 iterations, 0.4 mm pixel size, 0.585 mm axial). For dynamic analysis, data were re-binned into thirty 1 min bins. After 90 minutes rats were culled, tissues removed,

weighed and counted on a gamma counter alongside a serial dilution of the injected dose to allow the calculation of tissue uptake as percentage injected dose.

PET data were co-registered with the CT data and analysed using VivoQuant (inviCRO, Boston, USA). Volumes of interest were created for the heart, liver and kidneys and the %ID calculated for all at each time point.

Statistical analysis

Analysis was performed using GraphPad Prism® (GraphPad Software Inc, USA). All values are expressed as mean ± SD. All data were analysed using a one way ANOVA with Bonferroni correction post-hoc test or Dunnett's test when multiple comparisons were made to a control group.

Results

Figure 1 summarises the R_f values and log P values obtained for each ^{64}Cu-BTSC. Their lipophilicity increased linearly with molecular weight through alkylation at the R^{1-4} positions. Partition coefficients were unaffected by the use of KHB rather than water as the aqueous phase.

When perfusion was switched from normoxic to hypoxic buffer, afferent buffer O_2 saturation fell to less than 20 mmHg within 5 minutes, and to less than 5 mmHg by 25 minutes (Figure 3). The pO_2 of fully oxygenated KHB is approximately 500 mmHg, which saturated the Oxylite oxygen probes during normoxia (they have an operating maximum of 150 mmHg), but pO_2 decreased to measurable levels within a minute of switching to hypoxic buffer. Coronary perfusion pressure and left ventricular end diastolic pressure rose progressively from the onset of hypoxia. Developed pressure dropped rapidly, recovered briefly after approximately 15 minutes, before declining to zero after 40 minutes. Lactate release peaked at 0.78±0.3 nmol/min after 4 minutes of hypoxic buffer perfusion, before falling at a rate mirroring the decline in contractility. Creatine kinase leakage averaged

13

60±11 μU/min/g wet weight during aerobic perfusion, and did not increase during hypoxic buffer perfusion (data not shown).

BTSC complexes alkylated at R^1 and R^2 displayed decreasing normoxic tissue retention with decreasing lipophilicity (coefficient of determination = 0.84), with both ^{64}Cu-ATS and ^{64}Cu-CTS exhibiting less normoxic tissue retention than ^{64}Cu-ATSM (5.8±1.1 and 4.3±0.7 %ID versus 8.0±1.7 %ID) (Figures 4-6). During hypoxia, there was no relationship between tracer lipophilicity and tissue retention (coefficient of determination 0.41 and 0.24 after 5 and 25 min hypoxia respectively). After 5 min hypoxia, ^{64}Cu-ATS and ^{64}Cu-CTS both exhibited significantly greater contrast than ^{64}Cu-ATSM (9:1 and 10:1 versus 6:1 respectively), which increased further after 25 min hypoxia (14:1 and 17:1 versus 8:1 respectively).

^{64}Cu-PTSE and ^{64}Cu-PTSM (which are not alkylated at R^2) had significantly higher normoxic tissue retentions than the other tracers (54.5±3.5 %ID and 63.6±2.1 %ID respectively). They also displayed some hypoxia selectivity, with their tissue retention increasing to

14

86.2±7.5 %ID and 82.6.1±5.7 %ID after 5 min hypoxia, and 90.1±3.3 %ID and 89.5±5.2 %ID after 25 min hypoxia (p<0.05).

Tissue retention of ^{64}CuCl$_2$ was negligible regardless of the level of tissue oxygenation. ^{18}FMISO achieved a hypoxia:normoxia contrast of 5:1 after 25 minutes hypoxia; but first pass uptake was extremely low compared to the BTSCs (2.24±0.09 %ID).

During normoxia, the weight of the FCR for the R^1 and R^2 alkylated complexes was greater than 0.8, while for PTSE it was only 0.4±0.03. After 5 minutes of hypoxia, the weight of the FCR for the R^1 and R^2 alkylated complexes declined such that it was approximately equal to the weight of the SCR (while the weight of the FCR for ^{64}Cu-PTSE was still 0.76). By 25 minutes of hypoxia, the weight of the SCR had increased to 0.6 for all tracers. The weight of the SCR for ^{64}CuCl$_2$ was negligible in all cases. The SCR of the BTSCs was approximately 100 times smaller than the FCR during normoxia, and was comparable between ^{64}Cu-ATS, ^{64}Cu-CTS, ^{64}Cu-ATSM and ^{64}Cu-DTS (averaging 0.01±0.001 min^{-1}), while it was lower for the more lipophilic complexes (2±0.1x10^{-3} and 2.3±0.1x10^{-3} min^{-1} for ^{64}Cu-CTSM and ^{64}Cu-ATSE

respectively). The normoxic FCR of the BTSCs decreased (i.e. clearance was slower) with increasing lipophilicity, with ^{64}Cu-ATS (3.7 ± 0.2 min^{-1}) and ^{64}Cu-CTS (3.1 ± 0.3 min^{-1}) having markedly greater FCRs than ^{64}Cu-ATSM (1.2 ± 0.2 min^{-1}) (Figure 6). The FCR increased with hypoxic duration for all complexes except ^{64}Cu-PTSE. The FCR of ^{64}CuCl$_2$ was at least twice that of any BTSC complex (10 ± 0.7 min^{-1}), and decreased during hypoxia. It was not possible to calculate the FCR or SCR for ^{64}Cu-PTSM (or ^{64}Cu-DTSM during normoxia) because their clearance did not reach steady state. For the less lipophilic tracers, the SCR progressively fell with increasing duration/severity of hypoxia

In vivo, cardiac ^{64}Cu-ATSM, ^{64}Cu-CTS and ^{64}Cu-ATS retention fell to 0.6% of injected dose within 6 minutes of injection (Figure 7). ^{64}Cu-CTS retention within the heart averaged 0.54 ± 0.02 %ID over the last 20 minutes of the scan, significantly lower than ^{64}Cu-ATS (0.63 ± 0.2 %ID) and ^{64}Cu-ATSM (0.67 ± 0.01 %ID, $p<0.05$). This was confirmed by *ex vivo* biodistribution 90 minutes post-injection, where cardiac ^{64}Cu-CTS retention was significantly lower than the other two tracers (0.13 ± 0.02 %ID versus 0.25 ± 0.04 %ID for ^{64}Cu-ATSM and 0.24 ± 0.03 %ID for ^{64}Cu-ATS, $p<0.05$). The primary route of excretion of all three complexes

16

appeared to be hepatic, although both the imaging data and the *ex vivo*

biodistributions suggest that a larger fraction of ^{64}Cu-CTS clears renally.

Discussion

We have identified two complexes, ^{64}Cu-ATS and ^{64}Cu-CTS, which demonstrate greater hypoxic to normoxic tissue contrast, and superior pharmacokinetics (faster clearance from and lower retention in normoxic tissue) than the current lead hypoxia imaging agents ^{64}Cu-ATSM and [18]FMISO.

As has previously been shown in isolated cells[5, 9], we demonstrate that lowering the redox potential of ^{64}Cu-BTSC complexes by alkylating them at both the R^1 and R^2 positions results in greater hypoxia selectivity than ^{64}Cu-PTSE and ^{64}Cu-PTSM, which are only alkylated at one of these positions.[6] Our pharmacokinetic data show that the FCR is the primary determinant of BTSC kinetics in normoxic tissue, while the SCR dominates during hypoxia. This is consistent with a previous description of ^{99m}Tc-HL91 pharmacokinetics, which defines the FCR as an index of tracer washout through the vasculature, and the SCR as an indicator of tracer trapping.[23] As tracer washout increases with decreasing lipophilicity in normoxic tissue, reducing the lipophilicity of these complexes seems to be a useful strategy for improving their selectivity. ^{64}Cu-ATS and ^{64}Cu-CTS, which have a similar redox potential to [64]Cu-

18

ATSM, but which clear more quickly due to their lower lipophilicity gain significant advantage in terms of delivering greater contrast more rapidly after injection. They appear sufficiently lipophilic to cross cell membranes, but not lipophilic enough to be retained within them for a significant amount of time. This may also aid their tissue penetration by allowing them to diffuse further between cells without becoming detained in cell membranes close to the vasculature. The shift in dominant weights suggests that the importance of the FCR in governing tracer kinetics diminishes with increasing hypoxic severity, in favour of tracer trapping represented by the SCR. We currently interpret this shift as a reflection of the increasing "hypoxic fraction" of cells beyond the threshold for tracer retention in each case. It is interesting that the FCR appears to increase with increasing hypoxic duration/severity; we do not yet have an explanation for this.

In vivo, ^{64}Cu-CTS is retained less in normoxic myocardium than ^{64}Cu-ATSM, consistent with our isolated heart data. We are currently unable to perform ECG-gated preclinical PET imaging (which would enable us to distinguish myocardium from ventricular blood pool), but our *ex-vivo* biodistribution data confirm our PET data. The main non-target organs

that may confound myocardial hypoxia imaging are liver, lung and blood pool. Our data suggest that ^{64}Cu-CTS clears from these tissues faster than ^{64}Cu-ATSM (and equally quickly from blood), which may also enhance its utility, but it is unfortunately not possible to confirm enhanced renal clearance because we did not include bladder or urine samples in our biodistribution analysis.

While PET is unlikely to be the cardiologist's first choice for characterising ischemic myocardium immediately after an acute ischemic event in terms of speed, convenience or cost, we would suggest that this class of tracers exhibit unique potential in identifying chronic cardiac hypoxic syndromes such as those mentioned in our introduction which are more difficult to characterize by other means[3, 4]. It is an advantage of these tracers that they require biological reduction for their intracellular trapping, and as such are only retained within viable (and potentially salvageable) tissue[24]. It is not currently known whether these complexes all have the same sensitivity threshold with respect to *degree* of hypoxia; this is a critical consideration for their clinical utility, and will form the next phase of our evaluation of these complexes.

The biggest challenge to the development of this class of complexes now seems to be that while those currently available vary widely with respect to lipophilicity, they fall into only 3 groups with respect to redox potential[6]: ^{64}Cu-GTS and ^{64}Cu-GTSM have redox potentials at -0.43V vs Ag/AgCl, and are not hypoxia selective, ^{64}Cu-PTSM and ^{64}Cu-PTSE have redox potentials of -0.53V and -0.52V respectively, and are weakly hypoxia selective, while the rest of the complexes described here have redox potentials of -0.58V and -0.59V, and are selective for the extreme hypoxia that we induce in this heart model. It is likely that trapping is a balance between the dissociation rate of reduced complexes, and re-oxidation rate by oxygen, which have yet to be quantified.

^{64}Cu-PTSM has been previously investigated as a perfusion agent for monitoring myocardial blood flow,[25] on the assumption that its trapping is non-selective: its relatively low redox potential allows it to become reduced and dissociate in normoxic as well as hypoxic tissue[6]. Our data confirm previous reports that tissue retention of ^{64}Cu from ^{64}Cu-PTSM and ^{64}Cu-PTSE is also oxygen sensitive (though less so than the complexes alkylated at both R^1 and R^2). This suggests that either the reduction of these tracers by normoxic tissue is not maximal, or that a

proportion of the reduced complex may be re-oxidised by oxygen, allowing some tracer to escape the myocardium intact. Hypoxia either increases the efficiency of tracer reduction, abolishes the residual capacity for these tracers to be reoxidised, or both. Whichever is the case, their use as perfusion imaging agents should clearly be performed with caution.

To perform this work, we developed a "triple γ-detection" system to screen and characterise radiotracer kinetics and retention characteristics in isolated perfused rat hearts, which builds upon that previously described by Fujibayashi et al.[10] It allows the simultaneous monitoring of tracer input, cardiac retention, and washout in a beating heart model characterised in terms of contractility, arterial oxygen concentration, cardiac metabolism and viability. We have confirmed the extent of hypoxia induced by direct measurement of perfusion buffer oxygen saturation, as well as its biological impact. The onset of lactate production and lack of creatine kinase release confirms these hearts as biochemically compromised, but viable and potentially salvageable, which we believe represent an appropriate target for the first screening of these complexes.[3] Because of the rapid first pass kinetics of these

tracers, it was essential to obtain a true post-injection peak in the counts detected from the heart to enable accurate quantification of tracer retention as % injected dose.[22]   Boluses of ^{64}CuCl$_2$, our most rapidly clearing tracer, were registered in the heart detector within 3 seconds of injection, with a peak lasting 1 second. To ensure we were able to accurately capture the injection peak of all radiotracers, we therefore sampled at 5 Hz. In the future, we may be able to use the arterial line detector to provide an input function for more detailed pharmacokinetic models, but we are still developing this approach.

While hypoxia is a facet of ischemia, and the effects of the two phenomena are practically often difficult to resolve, they should not be used interchangeably[3]. We have specifically induced hypoxia in this experimental model because maintaining coronary flow constant greatly simplifies pharmacokinetic modelling. We demonstrate that these tracers respond to hypoxia, and it is established that ^{64}CuATSM responds in a similar manner the hypoxic component of the ischemic insult[24]. The extent to which the pharmacokinetics of these tracers is altered by other pathophysiological processes occurring during ischemia, such as waste product accumulation and acidosis, changes in

intracellular redox status, rapid depletion of energy substrates, and the effect of poor perfusion itself, remain to be fully characterised[3, 26].

The kinetic analysis used in this study has some limitations. The variability in the estimation of rate constants and their amplitudes increased as signal-to-noise ratio (SNR) decreased due to radioactive decay. It was also not possible to accurately estimate the SCR from tracers with very slow washout characteristics (such as ^{64}Cu-PTSM) within the time course of our current protocol. We therefore calculated tissue tracer retention as a percentage of injected dose after 20 minutes (as has been previously done[10]), rather than as the ratio between the SCR amplitude and the sum of the SCR and FCR amplitudes. While this introduces some time-dependency into our values, it also highlights tracers which wash out more completely by 20 minutes, which as we show here, is a desirable attribute. The observed relative shifts between FCR and SCR suggest that dynamic imaging and/or parametric mapping may be able to provide more detailed information on the behaviour of these tracers, and aid data interpretation. It may, for example, enable the correction of uptake values for perfusion, which has

been a consistent problem when interpreting hypoxia tracer uptake in tissue which is both hypoxic and flow-restricted.[27]

Conclusion

We have identified two complexes, ^{64}Cu-ATS and ^{64}Cu-CTS, which exhibit better pharmacokinetic properties and hypoxia selectivities than the current leading hypoxia imaging agents ^{64}Cu-ATSM and [18]FMISO. Their *ex vivo* pharmacokinetics and *in vivo* biodistribution confirm them as a potentially useful advancement of this class of compounds warranting further characterisation. The basis of this improvement is that decreasing the lipophilicity of these complexes, without altering their reduction potentials, improves their rate of washout from normoxic tissues and increases hypoxic to normoxic tissue contrast.

References

1. Sabbah HN, Sharov VG, Goldstein S. Cell death, tissue hypoxia and the progression of heart failure. *Heart Fail Rev* 2000;5(2):131-138.

2. Lanza GA, Crea F. Primary coronary microvascular dysfunction: clinical presentation, pathophysiology, and management. *Circulation* 2010;121(21):2317-2325.

3. Handley MG, Medina RA, Nagel E, Blower PJ, Southworth R. PET imaging of cardiac hypoxia: opportunities and challenges. *J Mol Cell Cardiol* 2011;51(5):640-650.

4. Sinusas AJ. The potential of myocardial imaging with hypoxia markers. *Semin Nucl Med* 1999;29(4):330-338.

5. Dearling JLJ, Lewis JS, Mullen GED, Rae MT, Zweit J, Blower PJ. Design of hypoxia-targeting radiopharmaceuticals: selective uptake of copper-64 complexes in hypoxic cells in vitro. *Eur J Nucl Med Mol Im* 1998;25(7):788-792.

6. Dearling J, Lewis J, Mullen G, Welch M, Blower P. Copper bis(thiosemicarbazone) complexes as hypoxia imaging agents: structure-activity relationships. *J Biol Inorg Chem* 2002;7(3):249-259.

7. Dearling JLJ, Lewis JS, McCarthy DW, Welch MJ, Blower PJ. Redox-active metal complexes for imaging hypoxic tissues: structure-activity relationships in copper(II) bis(thiosemicarbazone) complexes. *Chem Comms* 1998(22):2531-2532.

8. Lewis JS, McCarthy DW, McCarthy TJ, Fujibayashi Y, Welch MJ. Evaluation of 64Cu-ATSM in vitro and in vivo in a hypoxic tumor model. *J Nucl Med* 1999;40(1):177-183.

9. Handley MG, Medina RA, Paul RL, Blower PJ, Southworth R. Demonstration of the retention of 64Cu-ATSM in cardiac myocytes using a novel incubation chamber for screening hypoxia-dependent radiotracers. *Nucl Med Comms* 2013;34(10):1015-1022.

10. Fujibayashi Y, Taniuchi H, Yonekura Y, Ohtani H, Konishi J, Yokoyama A. Copper-62-ATSM: a new hypoxia imaging agent with high membrane permeability and low redox potential *J Nucl Med* 1997 1997;38(7):1155-1160.

11. Dence CS, Ponde DE, Welch MJ, Lewis JS. Autoradiographic and small-animal PET comparisons between (18)F-FMISO, (18)F-FDG, (18)F-FLT and the hypoxic selective (64)Cu-ATSM in a rodent model of cancer. *Nucl Med Biol* 2008;35(6):713-720.

12. Lewis JS, Herrero P, Sharp TL, et al. Delineation of hypoxia in canine myocardium using PET and copper(II)-diacetyl-bis(N(4)-methylthiosemicarbazone). *J Nucl Med* 2002;43(11):1557-1569.

13. Kositwattanarerk A, Oh M, Kudo T, et al. Different distribution of (2)Cu ATSM and (1)F-FDG in head and neck cancers. *Clin Nucl Med* 2012;37(3):252-257.

14. Lewis JS, Laforest R, Dehdashti F, Grigsby PW, Welch MJ, Siegel BA. An imaging comparison of 64Cu-ATSM and 60Cu-ATSM in cancer of the uterine cervix. *J Nucl Med* 2008;49(7):1177-1182.

15. Takahashi N, Fujibayashi Y, Yonekura Y, et al. Copper-62 ATSM as a hypoxic tissue tracer in myocardial ischemia. *Ann Nucl Med.* 2001;15(3):293-296.

16. McQuade P, Martin KE, Castle TC, et al. Investigation into 64Cu-labeled bis(selenosemicarbazone) and bis(thiosemicarbazone) complexes as hypoxia imaging agents. *Nucl Med Biol* 2005;32(2):147-156.

17. Blower PJ, Lewis JS, Zweit J. Copper radionuclides and radiopharmaceuticals in nuclear medicine. *Nucl Med Biol* 1996;23(8):957-980.

18. Oh SJ, Chi DY, Mosdzianowski C, et al. Fully automated synthesis of [18F]fluoromisonidazole using a conventional [18F]FDG module. *Nucl Med Biol.* 2005;32(8):899-905.

19. John EK, Green MA. Structure-activity relationships for metal-labeled blood flow tracers: comparison of keto aldehyde bis(thiosemicarbazonato)copper(II) derivatives. *J Med Chem* 1990;33(6):1764-1770.

20. Southworth R, Garlick PB. Dobutamine responsiveness, PET mismatch, and lack of necrosis in low-flow ischemia: is this hibernation in the isolated rat heart? *Am J Physiol* 2003;285(1):H316-324.

21. Urdal P, Stromme JH. Effects of Ca, Mg, and EDTA on creatine kinase activity in cerebrospinal fluid. *Clin Chem* 1979;25(1):147-150.

22. Ng CK, Sinusas AJ, Zaret BL, Soufer R. Kinetic analysis of technetium-99m-labeled nitroimidazole (BMS-181321) as a tracer of myocardial hypoxia. *Circulation* 1995;92(5):1261-1268.
23. Okada RD, Johnson G, III, Nguyen KN, Edwards B, Archer CM, Kelly JD. 99mTc-HL91 : Effects of low flow and hypoxia on a new ischemia-avid myocardial imaging agent. *Circulation* 1997;95(7):1892-1899.
24. Lewis JS, Herrero P, Sharp TL, et al. Delineation of hypoxia in canine myocardium using PET and copper(II)-diacetyl-bis(N4-methylthiosemicarbazone). *J Nucl Med* 2002;43(11):1557-1569.
25. Shelton ME, Green MA, Mathias CJ, Welch MJ, Bergmann SR. Kinetics of copper-PTSM in isolated hearts: a novel tracer for measuring blood flow with positron emission tomography. *J Nucl Med* 1989;30(11):1843-1847.
26. Dearling JLJ, Packard AB. Some thoughts on the mechanism of cellular trapping of Cu(II)-ATSM. *Nucl Med Biol* 37(3):237-243.
27. Wood KA, Honess DJ, Maxwell RJ, et al. Evaluation of the effects of blood flow on 64Cu-ATSM uptake in a rodent tumour model. *Clin Oncol* 2007;19(3):S50-S50.

Disclosures

None

Complex	R1	R2	R3	R4	Mol Weight	Rf (ITLC)	LogP (octanol/ water)	LogP (octanol/ KHB)
[64]Cu-ATS	CH_3	CH_3	H	H	293.86	0.7	0.88	0.91
[64]Cu-ATSE	CH_3	CH_3	C_2H_5	H	349.97	0.83	1.86	1.85
[64]Cu-ATSM	CH_3	CH_3	CH_3	H	321.91	0.79	1.69	1.72
[64]Cu-CTS	C_2H_5	CH_3	H	H	307.89	0.78	1.31	1.45
[64]Cu-CTSM	C_2H_5	CH_3	CH_3	H	335.94	0.82	1.97	1.94
[64]Cu-DTS	C_2H_5	C_2H_5	H	H	321.91	0.78	1.7	1.77
[64]Cu-DTSM	C_2H_5	C_2H_5	CH_3	H	349.97	0.85	2.01	2.02
[64]Cu-PTSE	CH_3	H	C_2H_5	H	335.94	0.8	1.74	1.68
[64]Cu-PTSM	CH_3	H	CH_3	H	307.89	0.74	1.52	1.56

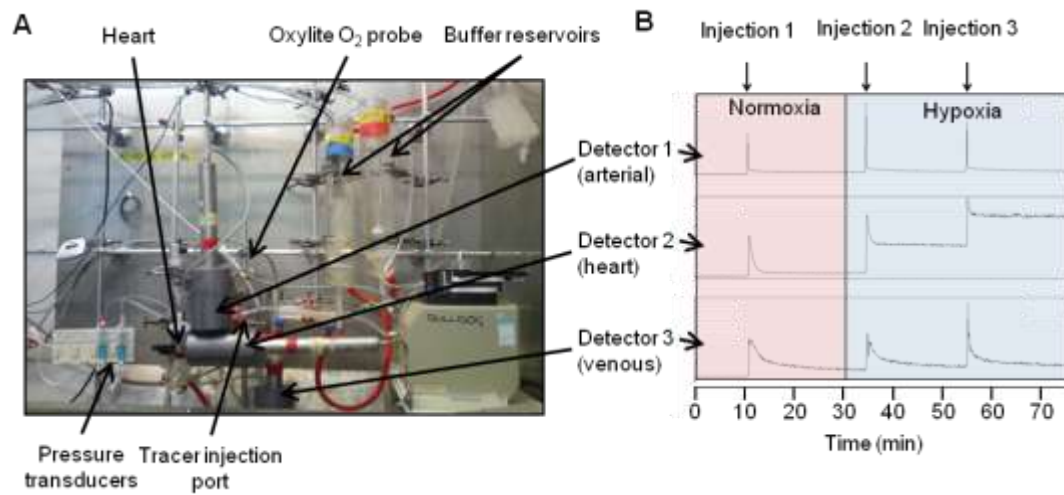Figure 1. Structure and physicochemical properties of the ^{64}Cu-BTSC complexes

Figure 2. (A) The triple γ-detector system for monitoring radiotracer passage the Langendorff heart apparatus. (B) Representative time-activity curves from ^{64}Cu-ATSM displaying the input function in the arterial line (detector 1), retention/washout through the heart (detector 2), and washout (detector 3).
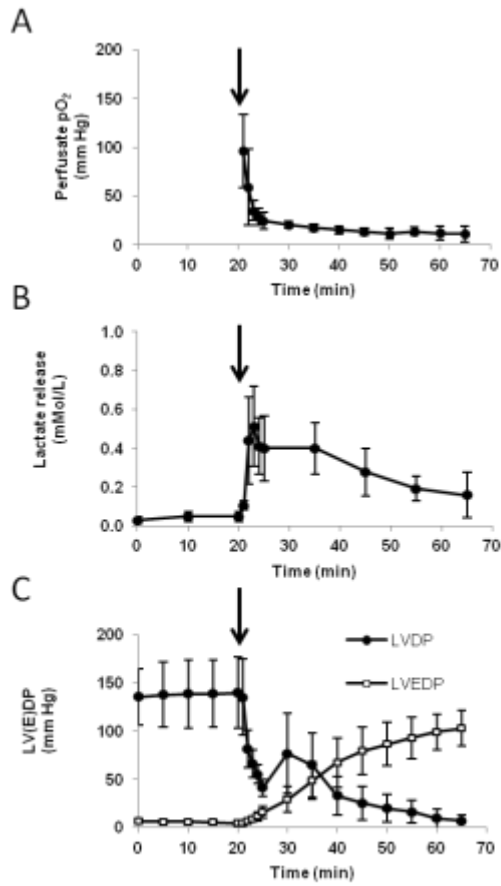
Figure 3. Hemodynamic data from isolated rat hearts during 20 minutes normoxic perfusion, then 45 minutes hypoxic perfusion (marked by arrow), showing changes in (A) perfusate pO_2, (B) left ventricular developed pressure (LVDP), (C) Left ventricular end diastolic pressure (LVEDP), and (D) lactate washout. Mean (n=5)±SD.
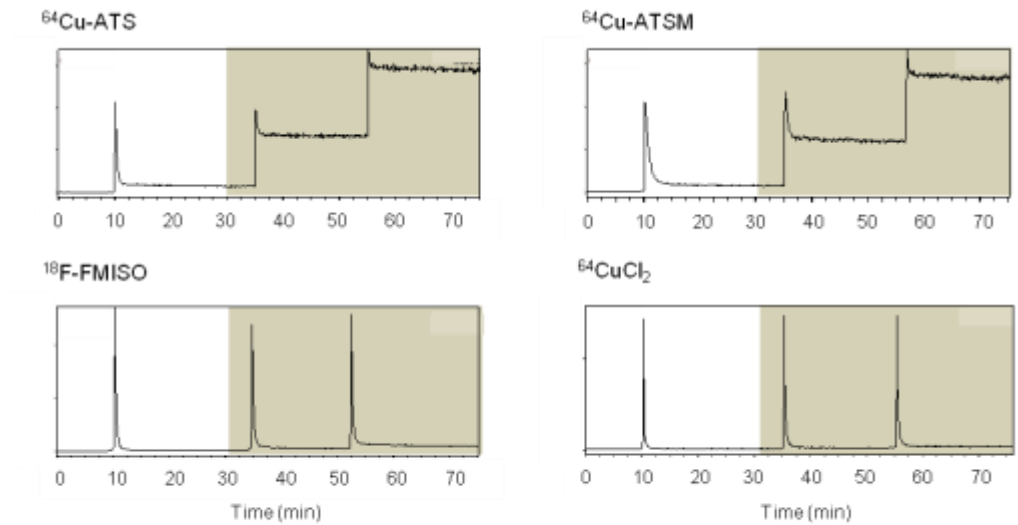
Figure 4. Representative time-activity curves showing the myocardial clearance/accumulation of ^{64}Cu-BTSCs, ^{18}FMISO and ^{64}CuCl$_2$ during normoxia (white background), and then hypoxia (grey background). Each spike represents a 1 MBq bolus.

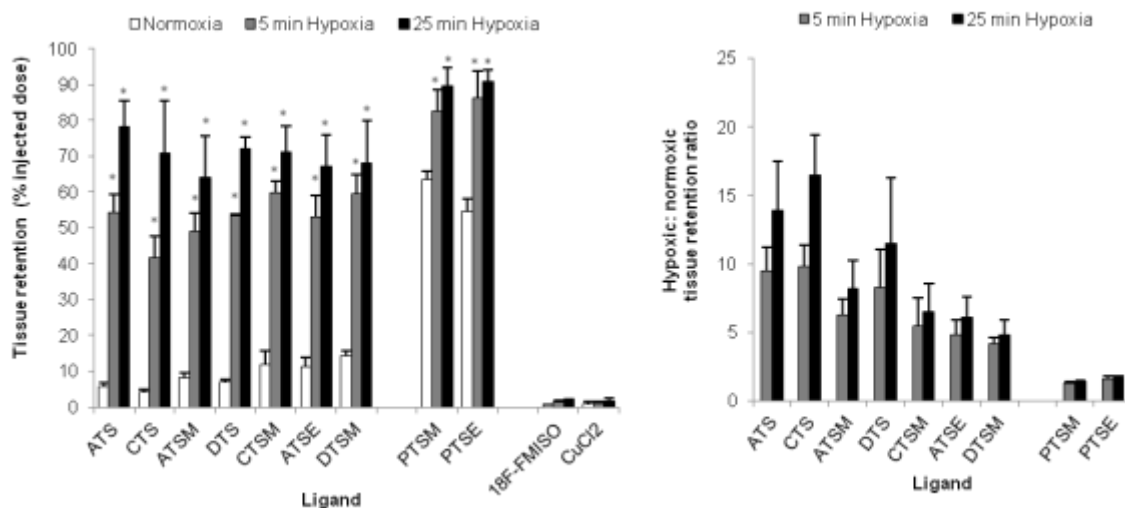Figure 5. (A) Tissue retention of ^{64}Cu-BTSC complexes, ^{18}FMISO and ^{64}CuCl$_2$ during normoxia/hypoxia. Asterisk indicates significantly different from corresponding normoxic control ($p<0.05$). (B) Normoxic:hypoxic contrast ratios calculated from (A). Asterisk indicates significantly different from corresponding ^{64}Cu-ATSM values ($p<0.05$). Mean ($n=5$) ± SD.
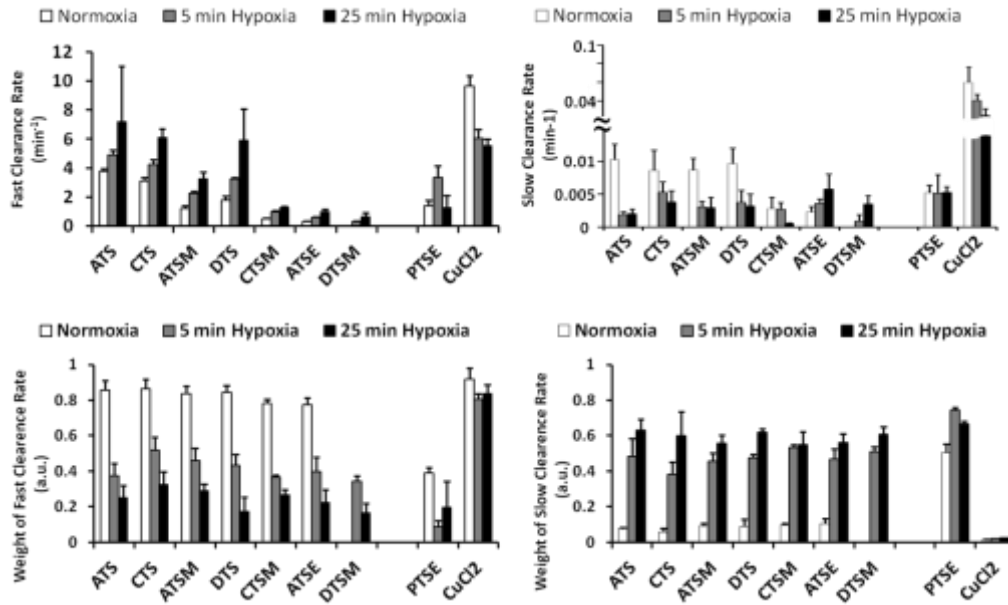
Figure 6. (A) Fast and (B) slow rates of tracer clearance from the myocardium (and their respective weights C & D). Data represent mean (n=5) ± SD.
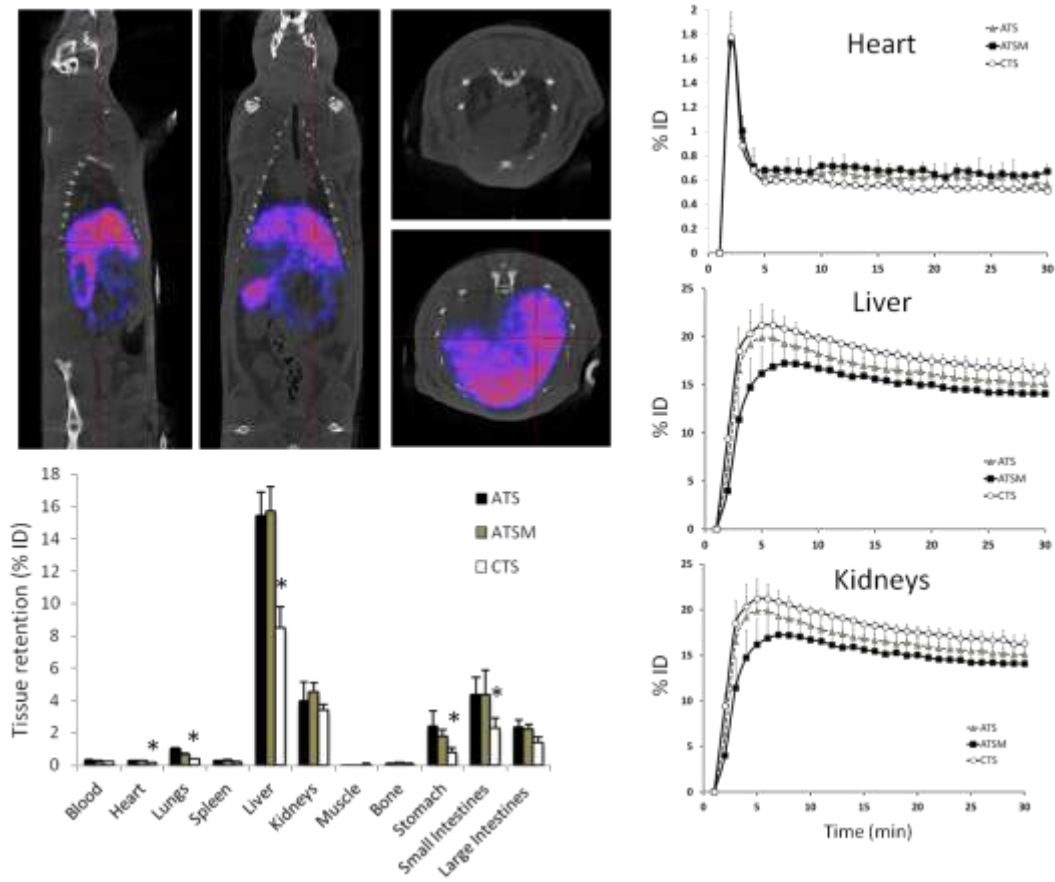
Figure 7. (A) PET-CT images of a healthy rat 30 minutes after injection with ^{64}Cu-CTS (5 MBq in 200 μL). (B, C, D) time activity curves showing tracer pharmacokinetics of ^{64}Cu-ATS, ^{64}Cu-ATSM and ^{64}Cu-CTS in heart, liver and kidneys respectively. (E) Tissue biodistribution of each tracer 90 minutes after injection. (n=3)±SD. Asterisk indicates significantly different from ^{64}Cu-ATSM (p<0.05).